Radio Frequency Backscatter Communication for High Data Rate Deep Implants

Ali Khaleghi, *Senior Member, IEEE,* Aminolah Hasanvand, Ilangko Balasingham *Senior Member, IEEE*

***Abstract*— In this paper, we study radio frequency (RF) backscatter for high data rate wireless communication with deep medical implants. The radar approach permits remote reading of the implant's information. This means the active transmitter is removed from the implant, that results in significant power saving. We customize our design for wireless capsule endoscopy (WCE) application, which is used for streaming high data rate video signals for improved visualization of the gastrointestinal tract. An efficient antenna system is designed and integrated into the WCE prototype that generates large radar cross section (RCS) using a self-resonant antenna geometry. The antenna is reconfigurable using an active micro-watt switch, which is controlled by the data stream. The switch alters the antenna RCS for an efficient modulation of the incident electromagnetic wave (EM) transmitted from outside the body. The antenna design considers the specific conditions of wave propagation in the biological environments and antenna loading with the lossy tissues. Polarization diversity using bi-static on-body reader antennas is used for communicating with the implant device. The on-body antennas can direct EM energy to the capsule device for improving the backscatter link performance. The feasibility study is demonstrated using numerical computations and experimentally validated in a liquid phantom and in-vivo animal experiments. A reliable backscatter data connectivity of 1 and 5 Mbps is measured for the capsule in the gastrointestinal tract for the depths up to 10 cm using an acceptable level of RF radiations.**

***Index Terms*—Antenna system, backscatter communication, implant antenna, biomedical applications, Wireless capsule endoscopy (WCE), Wireless communications.**

I. Introduction

ACTIVE wireless communication requires transceivers and the power resources for operation. Backscatter data telemetry is an approach that can eliminate the active transmitter from a device and save power, space, and cost. By using radio frequency (RF) backscatter, a remote reader can power up the data source of a tag device and the tag modulates the RF reflections back into the propagation channel for data communications. In this technique, the tag device remains passive and does not require the RF frontend for communications. Semi-passive tag device uses battery resources for activating the data source, and the communication is based on the backscatter technique. In the semi-passive tag, the communication range can be increased, and the tag can have more power resources for sensing and processing.

The well-known implementation of RF backscatter is radio frequency identification (RFID) [1]- [2] that communicates a specific code for the identification purposes. The communication can be realized using near-field coupling in low frequency (LF) or high frequency (HF) by implementing the coupling coils in which the range is several centimeters and the data rate is several Kbps; alternatively, the radiative fields in ultra-high frequencies (UHF) can be used for range extension to several meters and data rates of several tens of Kbps. Integration of sensors with RFID tag activates the technology for wireless sensor networks (WSN) for dynamic sensory data transmission [3]. The target applications are for the scenarios in which the active transmitter technology cannot be integrated into the tag device due to efficiency/power consumption balance while considering weight/size constraints. Using high data rate backscatter has significant potential for the future low power wireless connectivity. A short range, high data rate wireless backscatter communication in free space has been presented in [4]. We have demonstrated a long range (10-15 m) backscatter communication for image data transmission [5], and a battery-free video streaming using RF backscatter and power harvesting was presented in [6].

An important application of the RF backscatter is for the biomedical implant sensors in which the physical access to the implant is restricted, and the battery resources are limited due to the nature of the implant device. The wireless backscatter technology might enable internet connectivity to the bio-implant sensors [7]. This means it can have a significant impact on the future implant technology.

The backscatter communication with an implant is different from a device operating in free space. This is due to the different

The paper submitted on July 2018. The work has been supported by the EU's H2020: ITN:MSCA:WIBEC project (grant no. 675353) and the Research Council of Norway projects "High data-rate wireless communication for deep medical implants" (grant no. 282110) and "Wireless In-body Sensor and Actuator Networks" (grant no. 270957). The antenna is a part of the patent "Medical Implant with Wireless Communication", application no. 62201-15239-GB-1, 2016.

Ali Khaleghi is with Intervention Center, Oslo University Hospital, Oslo Norway, and Norwegian University of Science and Technology (NTNU), Trondheim, Norway, alli.khaleghi@ntnu.no.

A. Hasanvand is with the electrical engineering department of K.N. Toosi University of Technology, Tehran, Iran. I. Balasingham is with Intervention Center, Oslo University Hospital, Oslo, Norway and the Norwegian University of Science and Technology (NTNU), Trondheim, Norway, Ilangko.balasingham@ntnu.no.

wave propagation nature in the biological tissues, radiated power limitations and the implant size restrictions in which the communication range and data rates are significantly reduced. RFID technology for the medical implant connectivity has been studied previously in which a limited communication range and data rates were reported [8]- [12]. Using magnetic induction at LF and HF can provide wireless power transfer (WPT) and data telemetry for superficial implants located in a few centimeters of depths [13]- [14]. The magnetic field indicates less loss in the biological tissues, but it is further limited to the reader coil proximity and is highly sensitive to the relative orientation of the reader and implant coils. Thus this limits the read range of the device [10]; in addition, the data rate is limited by the narrowband nature of the magnetic induction system. Using propagation modes in UHF frequencies, one can increase the read range of the device. Moreover, larger bandwidth can be used for high data rate connectivity because more efficient antennas with less sensitivity to the orientation can be realized. However, the communication range is limited by the wave propagation loss in the biological environment. This leads to a shorter reader range achieved considering the RF safety requirement imposed by the specific absorption rate (SAR) [15]- [16].

Using backscatter for high data rates sensory systems such as neurological implants and wireless capsule endoscopy (WCE) is a feature for future medical technologies. The requirement for these devices is continuous or real-time data transmission, within depth inside the body, which is not feasible by using the active transmission approaches. In this paper, for the first time, we address using backscatter communication for high data rate deep implants, such as for WCE with continuous data/video streaming. The proposed RF backscatter uses a semi-passive approach in which the sensory system or camera powers by an onboard battery and the wireless communication is based on the backscatter technique. The RF frontend in the capsule device is replaced with a micro/nano watt electronic switch. This means the power consumption of a typical active transmitter, which is in the order of 20-45 mW can be eliminated. Thus continuous high data rate, real-time video streaming without reducing the lifetime of the device can be enabled. Our approach is mainly focused on the antenna system design for the implant and the reader system in which we use the near-field characteristics of the reader antenna in UHF band to increase the communication range. To accomplish the antenna design, the knowledge of EM wave propagation in the biological tissues, small antenna design for efficient RF reflections, and interaction of antennas with the biological environment are used to improve the communication system efficiency for providing connectivity in depths greater than 10 cm. In our design, the capsule length is 20 mm (the integrated antenna length is about 10 mm), and the diameter is less than 10 mm to fit into a swallowable shell. The frequencies used for the data communications must be in the regulated medical bands and should have a low loss in propagation through the human organs. Also, the RF radiation safety must be considered in the design process.

The paper is organized as follows. In Section II, we discuss the limitation of small antennas and their usage in the biological mediums. In Section III, the key design considerations for implant backscatter antenna is discussed. In Section IV, the antenna design and analysis with integration for backscatter WCE system are presented, followed by the on-body reader antenna design and configuration in Section V. The link simulations and the reader antenna requirements are analyzed in Section VI. The backscatter antenna simulation, measurements in a liquid phantom and in-vivo animal experiments are provided in Section VII. Section VIII is the discussion and conclusions.

II. Small Antennas in Biological Tissues

The biological tissues contain significant water and minerals that impose high permittivity and conductivity into the medium. These material properties are frequency dependent and have been measured primarily by Gabriel [17]. The tissues with high water contents indicate high permittivity values. Depending on the minerals, the tissues can have different conductivities. The conductivity increases for higher frequencies and is the source of electromagnetic wave attenuation through transmission in the biological medium. Fig. 1 shows the permittivity and conductivity of selected tissues (muscle, fat, intestine, bones and blood) in the frequency range of 100 to 3000 MHz. The conductivity is smaller for low frequencies, so is preferred for signal transmission inside the biological tissues due to the amount of the loss. The permittivity is high for the tissues with higher water contents.

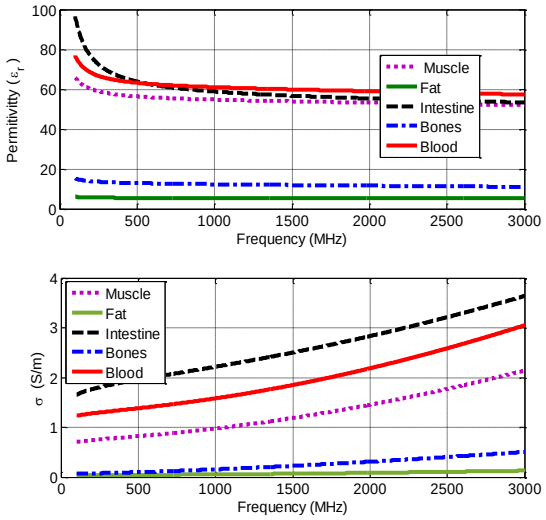

Fig. 1 Conductivity and permittivity versus frequency for the sample biological tissues of muscle, fat, intestine, bones and blood.

In a communication system, the antenna is a part of the transmission path and plays a crucial role on EM wave coupling to/from the medium. Thus the combined effects of the antenna and the material loss constitute EM wave coupling between transceiver devices in the biological environment.

The main limitation with the antennas is the size constraint and the antenna usage inside the lossy biological tissues. The implant device should be small enough to be implanted permanently or temporally for medical sensing and actuation. Also, the antenna should hold a specific planar or conformal geometry depending on the application scenarios such as WCE,

leadless pacemaker or wireless neuronal implants.

The frequency regulatory body also has a definition for the frequencies which can be used for the medical sensing. FCC and ITU define these frequencies while some countries have their standards [18]-[20]. The medical frequencies are placed in the bands at 400, 600, 800, and 1400 MHz due to their availability, loss characteristics in the biological medium and the applications from the medical sectors [21]. Considering the implant's physical size, maximum 35 mm, and the recommended frequencies, the normalized implant size is usually less than $0.05\ \lambda \sim 0.16\lambda$ (λ is the wavelength in free space) for the above mentioned upper and lower frequencies. Reminding that a part of the device size is assigned for the antenna integration, the available space for the implant antenna is much less than the size mentioned above. WCE is used in the small intestine and has a cylindrical shape with the available antenna length of 10 to 15 mm and a diameter of about 9 mm.

Small antennas in free space have been thoroughly investigated [22]. The main character of these antennas is the significant amount of the reactive field nearby the antenna structure. This causes a high amount of coupling from the antenna to the surrounding environment. Thus, the presence of any lossy material, cable or electronics in the close perimeter of the antenna alters the current distribution on the antenna structure and makes the antenna impedance and radiation character more susceptible to the surrounding medium. Furthermore, the small antenna radiation resistance is very small making it difficult to tune the transmitter/ receiver device without significant loss in the matching network. Even, by using a suitable matching, the current flow on the antenna structure can be high. Thus more considerable ohmic losses reduce the radiation efficiency.

Using small antennas immersed in the biological medium is further limited, due to the strong near-field of the small antennas and the close perimeter to the lossy medium; therefore, significant loss by the near-field loading is inevitable. The loss effect can be observed in the antenna input resistance (R_{in}) as the ohmic resistance (R_Ω) added to the antenna radiation resistance (R_r), i.e., $R_{in}= R_\Omega+R_r$. As R_r is very small for small antennas and R_Ω is significant due to the material loss, therefore the embedded antenna input resistance (R_{in}) is managed by the loss. The ohmic resistance might be reduced by holding a gap between the metallic antenna structure and the surrounding medium to detach the antenna near-field from the lossy environment. However, the added space reduces the space for the antenna. We have investigated the gap around the antenna for the conceptual antennas, loop and dipole, and we found that a minimum air space of 0.5 mm around the antenna is required to keep the antenna radiation efficiency as maximum as possible. The larger gaps have less effect on the antenna efficiency and reduce the antenna's physical space. Overall, it is required to increase the radiation resistance of a small implant antenna for efficient operation with less influence from the surrounding lossy medium. This consideration is carried out in our antenna design.

We note that designing a high efficient antenna may not be a critical requirement for the systems with active transmitters, considering the design complexity and the size requirements. The reason is that increasing the transmitter power in some extends can compensate for the low antenna efficiency. The assumption is that the significant part of the DC power is used to run the local oscillators and modulator of an RF frontend rather than the RF power amplification, i.e., increasing the RF power level by some dB will slightly increase the percentage of the system DC power consumption.

For the backscatter usage, the antenna efficiency plays a crucial role in the communication link performance. It is challenging to compensate the poor antenna efficiency by transmitting a considerable amount of power from the external reader, which has to abide by the spectral emission limitations and RF safety issues.

III. Backscatter Antenna for Implants

In a backscatter communication system, the wave propagation is conducted in round way from the reader to the tag device. The operation principle is that the amplitude/phase of the incident wave is altered by the tag antenna switching in a way that the antenna reflections are modulated. The data source controls the wave reflections; thus the reader can extract the tag's information. In the backscatter link, the antenna radar cross section (RCS) is considered as the primary way of carrying communication signals in which the antenna gain and efficiency are applied for both reception and re-radiation modes.

RCS calculations for plane wave illumination and aperture antenna assumptions for the tag has been provided [23]- [24]. Also, the RCS depends on the load connected to the tag antenna and the structural mode (As) which has a load-independent antenna factor [24]. The Thevenin equivalent circuit model is proposed for the minimum scattering antennas (MSA) which provides RCS as [23],

$$\sigma = \frac{\lambda^2 G^2 R_a^2}{\pi |Z_a + Z_{load}|^2} \qquad (1)$$

where λ is the wavelength, G is the antenna gain in the same direction of the incident EM wave, $Z_a= R_a+jX_a$ is the complex radiation impedance of the antenna and Z_{load} is the antenna's load impedance. For backscatter communication, the modulation vector is essential to discriminate among the data signals [24]-[25]. It is specified by the differential RCS (ΔRCS) vector of the antenna. The ΔRCS can be managed by altering the antenna reflections using different antenna loads [25]- [27].

In a passive RFID tag, the RF signal is used in a rectifier diode circuit, and the energy is stored in a capacitor for the system operation. For an RFID integrated circuit (IC), Z_{load} is the IC input impedance. For maximum power transfer, the antenna impedance must be conjugately matched to the IC impedance. With the conjugate matching, ideally, half of the power is delivered to the load and half is reflected into the antenna. For backscatter data communications, maximum reflections (1) are required, that can be attained with Z_{load}=0, in which RCS value depends on the antenna complex impedance ($Z_a= R_a+jX_a$) [23]. Based on (1), the maximum reflection is

obtained in the resonance frequency of a self-resonant antenna (X_a=0) using the short circuit load impedance (Z_{load}=0), or by using a pure imaginary conjugate matched load (Z_{load}=-jX_a).

Using the passive tags with a matched load for wireless power transfer and a short circuit for maximum reflections, the ΔRCS is reduced due to the power reflections from the matched load. For a semi-passive tag device, the power transfer is not the system operation task, and the device's data source is activated using an onboard battery. Therefore, the antenna impedance match is not required, and open circuit (Z_{load}=∞) is used to minimize the antenna reflections, or a load impedance can be optimized to provide maximum reflection with a tuned phase for maximum ΔRCS vector [24]. The procedure for finding the optimized antenna load impedances for a semi-passive tag in free space is provided in [24].

Using the backscatter for the implant communication is different from the free space. The reader signal must penetrate inside the human subject, the permittivity of the human body is high compared to the air interface. Thus significant impedance mismatch occurs by wave propagation from the free-space to in-body [28]. Using the reader antennas in proximity to the body surface can reduce the mismatch effect for better EM wave coupling into the body. In this usage, the communication is limited to the view angles of the on-body reader antennas. Using bi-static reader, the reader antennas should be held close to the tag antenna in the common coverage area for successful communications. High coupling between antennas would prevent a successful data reading because of the transmitter signal leakage into the receiver that limits the dynamic range of the receiver and can cause the receiver saturation. This will require using polarization and space diversity to interrogate with the implant device to minimize the coupling. Moreover, the implant device is in several centimeters depth and operates in the medical frequencies thus the tag device remains in the reader's near-field region. Therefore, the aperture antenna assumption used for the RCS calculation in (1), the same far field antenna gain in the forward and backward paths and the plane wave assumption are not entirely valid for the implant backscatter antennas.

The small antennas have little radiation resistance and are highly reactive. The lossy medium dissipates the reactive field as heat in the proximity of the antenna which appears as an ohmic loss in the antenna input impedance. The amount of the ohmic loss is significant compared to the low radiation resistance (R_r) of the small antenna. Thus the equivalent Thevenin model (1) shall consider the ohmic loss for the implant backscatter case. Furthermore, the implant antenna impedance is sensitive to the antenna loading with the surrounding biological medium in which a fixed value of loading for WPT or backscatter cannot be considered for providing maximum RCS.

Due to the issues mentioned above and different usage conditions compared to the free space, the backscatter communication formulas might be revised for the implant usage. In this paper, we mainly focus on the engineering solutions and designs using computational electromagnetics approach rather than the analytical analyses.

IV. Implant Antenna Design

Radiation efficiency of an antenna depends on the antenna's physical size and dimensions compared to the wavelength [22]. The swallowable WCE has a maximum length of 25 mm and a diameter less than 10 mm; it travels through the human gastric tract and transmits the captured pictures/video to an external body device for the visualization of the small or large intestine for diagnosis. The available space for our antenna is 10-12 mm in length and 9 mm in diameter, where the rest of the space is allocated to the camera, light source, electronic boards and the batteries. The antenna is encapsulated in a biocompatible shell. The WCE device can be accessed from the belly within the depth of 10 cm from the front body, and deeper depths (if required) may be accessed from the back side of the body.

Due to the round way path loss through the biological tissues, the effect of the antenna gain and efficiency in both the reception and re-radiation modes and to establish a reliable communication link with reader antennas, a precise antenna design for backscatter must be considered. This requires a self-resonant antenna to maximize the wave reflections, and a semi-passive backscatter approach to increase the discrimination between the wave reflections, ΔRCS.

The maximum available space is used to achieve the maximum antenna efficiency. A planar conformal antenna that can be integrated into the perimeter of a cylindrical capsule device is designed. Therefore, the antenna interior space can be used for the integration of the other electronics to save the space. The target frequency band of operation is placed at 608-614 MHz which is allocated for the Wireless Medical Telemetry Service (WMTS). By considering the wavelength, the maximum antenna length is 0.02 λ at 600 MHz band. For the given antenna size, operating at the lower medical frequency bands around 450 MHz reduces the antenna's normalized size (0.015λ), and thus the antenna efficiency is further reduced. Using frequencies above 800 MHz, even increase the antenna normalized size (0.026λ), indicates more EM wave loss by transmission through the biological medium due to the increased conductivity of the tissues. Thus more loss/cm results. In conclusion, the operating frequency must be compromised in relation to the antenna size in which there will be a range of frequencies that can provide maximum radiation efficiency of a biologically embedded antenna.

The general form of the antennas are dipole and loop configurations in which the dipole antenna has an open current path, and a loop antenna constitutes a closed current path. The loop antenna has an intense magnetic near-field which dissipates much less power to the surrounding tissues than the dipole antennas with a strong electric field. Thus a small loop antenna results in better efficiency in the biological tissues [29]. The reason for improved efficiency with the loop antennas is the magnetic permeability of the biological tissues that is lossless (μr=1). However, the electric permittivity is lossy (complex εr). The main problem with using small loop antennas is the substantial current flow on the antenna surface due to the small radiation resistance. This means the antenna ohmic loss reduces the efficiency. Here, we start the design with a meander-shaped loop antenna geometry to reduce the near field

loss in the biological tissues. Then the antenna feeding is modified to generate a self-resonant geometry with a tunable input resistance for an improved antenna efficiency in the biological tissues.

The designed meander loop antenna has several bend lines and is connected to the feed ground to constitute a closed current path (Fig. 2(a)). The planar antenna is used in a cylindrical conformal geometry to be integrated into a WCE device (Fig. 2(b)). The vertical meander lines are 11.5 mm, the horizontal lines are 2 mm, and the path width is 0.5 mm. The antenna material is in Copper with the conductivity of σ=5.8×107 S/m and thickness of 35 microns. The antenna is integrated inside a capsule shell of permittivity (εr=4.3, σ=0.0054) with a gap of 0.5 mm to the shell and the shell thickness of 0.5 mm. The simulation model includes a metallic cylinder underneath the meander antenna to simulate the battery and the other electronics effects (Fig. 2(c)). The initial simulation, modeling, and parametric analysis were conducted in the homogenous biological tissue of single layer muscle as the basis for our calculations. Frequency-dependent material property of the muscle is considered in the simulations. The final design and implementation use the heterogeneous anatomical model of the human body and animal experiments. Fig. 2(d) shows the simulation model inside a muscle sphere of radius 10 cm. The numerical electromagnetic computations are conducted using CST Microwave Studio (MWS) using Time domain and the Frequency domain solvers to compare the accuracy of the computations for the small structure. Close agreement between the simulations can be achieved by using high-density mesh in the time domain solver using the local mesh options. The frequency domain solver is more accurate for the small size structures but cannot be used in the simulations with the human body anatomical model using the Voxel data.

The simulated antenna impedances (real and imaginary) in the muscle tissue is shown in Figs. 3 (a), (b). The imaginary part of the impedance can be separated into two regions. Frequencies below 700 MHz, in which the antenna reactance is inductive, and above 700 MHz, in which the reactance is capacitive. The antenna input resistance can be expressed as, $R_{in}=R_r+R_c+R_m$, where R_r is the radiation resistance, R_c+R_m is the ohmic loss resistance (R_c is the conductor loss, and R_m is due to the biological material loss). In the transition region at 700 MHz, the antenna behaves as an open circuit with high input resistance, and the antenna input resistance reduces above and below the transition region, in which the conductor loss and material loss are negligible compared to the high radiation resistance, i.e., the antenna input resistance is mainly managed by the radiation resistance. For the frequencies far from the transition region, the antenna resistance is dominated by the loss resistance, i.e. $R_r < R_c+R_m$. By using the meander loop geometry, we can realize an antenna with a wide range of input resistances from several ohms to several kilo ohms in different frequencies. The antenna requires a matching circuit in any frequency in the range for optimal operation with resonance.

To minimize the effect of the antenna medium (ohmic loss resistance) in the antenna input resistance, for an efficient

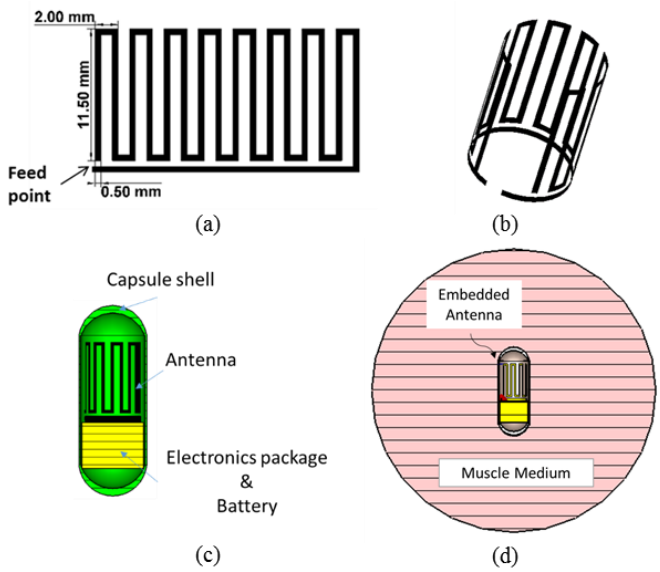

Fig. 2 Meander loop antenna geometry a) planar b) conformal cylindrical geometry c) integrated antenna inside a glass shell d) simulation scenario, muscle embedded antenna

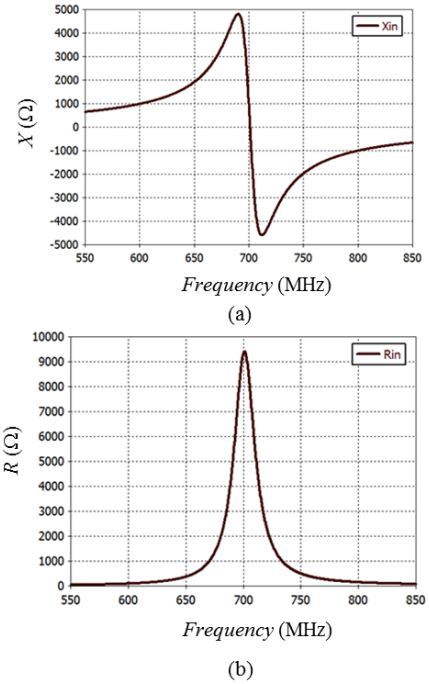

Fig. 3 Meander loop antenna input impedance a) imaginary b) real

radiation, we can operate in a frequency in which the radiation resistance is much larger than the loss resistance, so more significant part of the source power can be delivered to the antenna for radiations and less current paths through the circuit for reduced ohmic loss. We note that the antenna input resistance cannot be substantial (kilo-ohm range) that might prevent the current flow along the antenna structure that is applied by the source signal. Therefore, it is essential to select an appropriate frequency of operation with a moderate input resistance (30-200 ohms).

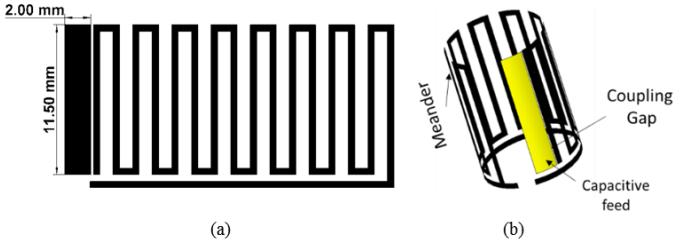

Fig. 4 Meander loop antenna geometry with parasitic patch feed a) planar b) conformal cylindrical geometry. Patch length= 11.5 mm, patch width=2 mm, meander trace width= 0.5 mm, line spacing 1 mm.

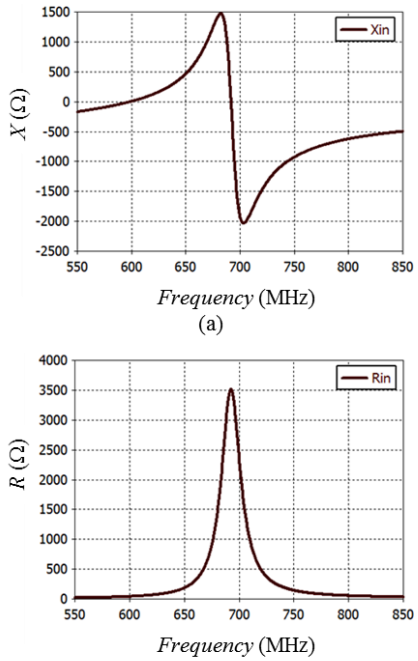

Fig. 5 Input impedance for the capacitive feed meander loop antenna inside muscle sphere a) imaginary b) real; the antenna resonances at 600 MHz with R_{in}=36 ohms.

It is required to provide a resonance frequency in the frequency region in which the radiation resistance is larger than the loss resistance to realize an efficient antenna for the backscatter. Also the incident wave/ source signal must generate the current flow along the antenna structure. For this purpose, a capacitive section is added to the meander antenna as shown in Fig. 4 using a patch monopole antenna. The patch is very small compared to the wavelength, and provides high capacitive reactance. By coupling the patch capacitance via a gap to the meander section, and by measuring the antenna input impedance from the patch feed point, the antenna self-resonance occurs by shifting down the inductive reactance of the loop in Fig. 3(a), as shown in Fig. 5(a). Fig. 5 shows the real and imaginary parts of the capacitive feed antenna in the muscle sphere using a coupling gap of 0.2 mm (see Fig. 4(a)). The gap to the meander section manages the coupling coefficient. The patch length manages the capacitance value. The overall effect is that the capacitive reactance of the patch removes the inductive reactance of the loop, and this generates a resonance frequency. The amount of the capacitive reactance defines the resonance frequency in which the antenna input resistance can be defined. Therefore, depending on the capacitive reactance, the resonance can be tuned in any frequency from 500 to 700 MHz with different antenna resistance. As the antenna normalized size and material loss changes slightly in the frequency range, the variation on the input resistance of the antenna is mainly related to the radiation resistance. The optimum operating frequency for the backscatter is the resonance frequency in which the antenna input resistance is much larger than the ohmic resistance for maximum backscatter with reduced effect of the surrounded tissues.

For the backscatter communication in the biological tissues, the patch is connected to an RF switch which is controlled by a serial data source. The switch connects/ disconnects the patch to the RF ground strip. By providing the closed path in the circuit, the antenna resonance is generated, and the maximum power from the incident field to the antenna is delivered. Short circuit state is used to re-radiate the maximum absorbed power into the biological medium. The open switch disconnects the resonance circuit, and with no resonance state, the minimum reflections from the antenna circuit are provided. The antenna operating frequency is tuned at 604 MHz with an input resistance of 40 Ω, of which the ohmic resistance is calculated 10 Ω.

Using Thevenin equivalent circuit approximation (1), we can define the antenna input impedance as $Z_{in} = R_r + R_\Omega + jX_{in}$ and Z_{load} is {0 or ∞} for the short/open states of the switch, respectively. We observe that in the resonance frequency, $X_{in} = 0$, with, $Z_{load} \approx 0$, the maximum reflection occurs by minimizing R_Ω relative to R_r of the antenna. Therefore, it is essential to tune the antenna operating frequency within region $R_r \gg R_\Omega$. However, larger R_r limits the current flow in the antenna structure for an applied incident electric field. Also as ΔRCS is used as the basis for data modulation, using large R_r performs similar to the open circuit switch state with low current and thus no modulation would occur with switching. A compromise between efficient reflection for large RCS and high ΔRCS must be considered to achieve optimal operation for the backscatter. The patch length and gap to the meander section are used for adjusting the optimum backscatter frequency in the predefined design frequency.

V. On-body reader antenna

The bi-static radar approach is used to read the capsule endoscopy data. The reader antennas are attached to the body surface to couple EM wave into the body toward the implant antenna. As the distance from the reader antenna to the implant is several centimeters and the antenna coverage angle is limited, the implant antenna must be found in the view angle of the reader antenna. Therefore, it is required to use an array of reader antennas on the body surface and switch among the array elements for an efficient coverage over all the digestive tract. Also, the bi-static reader antennas must be placed in the proximity to each other to transmit and receive the backscatter signals in the antenna coverage region. Using small distance between the antennas causes significant coupling that reduces the dynamic range of the receiver and might cause the receiver

saturation. This may lead to signal distortion in the receiver. Polarization diversity is used to control the coupling level between the reader antennas.

Different antennas are designed and tested for an efficient EM wave coupling to the biological medium. A 3D spiral antenna has been proposed in [30], and a liquid matching layer has been used to compensate the mismatch between air and the biological medium [28] for an efficient EM radiation from outside to inside the body. Even if the antenna could provide circular polarization, but the large size of the antenna prevents the use of the antenna for practical implementations on the body surface. Planar antennas are preferred that can be integrated into a belt type reader and can be installed on the body surface. A simple antenna is used in this paper that can provide an adequate reading range. The antenna has a meander loop geometry to increase the electrical length of the loop geometry for impedance matching at 600 MHz band. The loop antenna can provide more efficient EM wave coupling to the body and quite uniform coverage area along the loop center region. Fig. 6 shows the meander loop antenna geometry optimized with a gap of 1 mm to the underneath tissues layer.

Fig. 7 shows the simulated E-field generated by the meander loop antenna in the muscle tissues. As shown, the E-field is maximum along the loop center line in the tissues. A part of the antenna radiation is in the free space. This radiation might be reduced by using a back metal plate or a back cavity.

The simulated and measured return loss versus frequency is illustrated in Fig. 8. The measurement is conducted on the abdomen surface of a human subject and on a liquid phantom mimicking the material properties of the average body at 750 MHz in which a standard phantom is realized. The phantom is realized using combinations of water (55.42%), salt (1.3%) and 1,2-Propanediol (43.3%) to mimic the average material properties of the body tissues at 750 MHz [31]. The liquid is used for our test at 600 MHz in which we expect small changes with the 150 MHz shift in the operating frequency. There is an excellent agreement among the results. The difference is due to the different average material properties of the tissues used in the simulation and measurements.

As a guideline for maximum applicable power for the reader antenna, the SAR is computed. The calculated SAR (10g) is 10 W/kg for 1 W of the applied power. Considering SAR (10g) limit of less than 2 W/kg the maximum applicable power is limited to 200 mW for continues radiations. We note that SAR (10g) < 2 W/kg is defined as the maximum for head exposure for mobile telephone applications. For the medical usage and partial body except head exposure SAR (10g) < 10 W/kg can be considered based on IEC 60601-2-33. Thus maximum power of 1 W can be applied.

VI. Coupling between Implant and On-Body Antenna

The coupling link between the implant capsule antenna and the on-body antennas is computed for two orthogonal polarizations of the meander loop. Both the implant capsule and the on-body antennas are perfectly matched to the source impedance at 600 MHz. Fig. 9(a) shows the simulation model, in which the capsule is inside the muscle box, and the meander

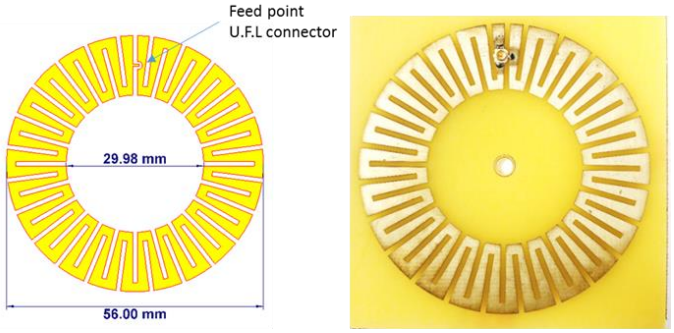

Fig .6 Meander loop antenna geometry used as the reader antenna a) simulation model b) manufactured antenna on a flexible substrate of thickness 0.1 mm

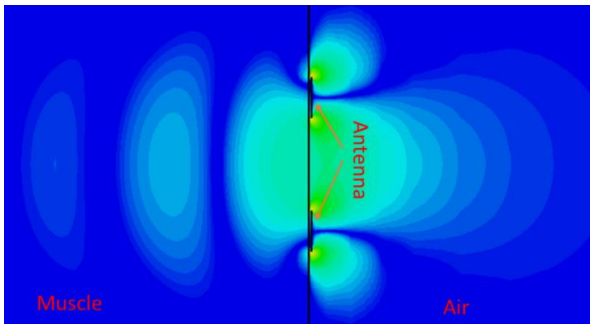

Fig. 7 E-field intensity in the muscle tissue and air at 600 MHz using the meaner loop antenna geometry

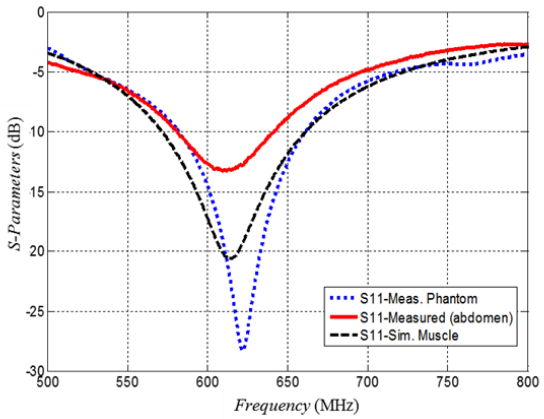

Fig. 8 Measured and simulated S-parameters of the on-body loop antenna. Measurements are conducted on the abdomen of a human subject and liquid phantom; Simulations are conducted on a muscle box

loop is on the muscle surface with a gap of 1 mm to the muscle. The boundary on the loop side is open, and the rest of the boundary is connected to the muscle tissue to extend the simulation domain of the muscle medium to infinity. Thus, the wave propagation to the tissues is considered from the loop antenna direction. The coupling link for the capsule within the depth of 50 mm is shown in Fig. 9(b). As shown, almost equal coupling (-32 dB) for both orientations of the loop antenna is obtained. As the electric field of the meander loop antenna inside the muscle tissue is purely linear polarized, we can conclude that the capsule antenna radiates in two orthogonal polarizations with almost equal ratios. This makes it easy to

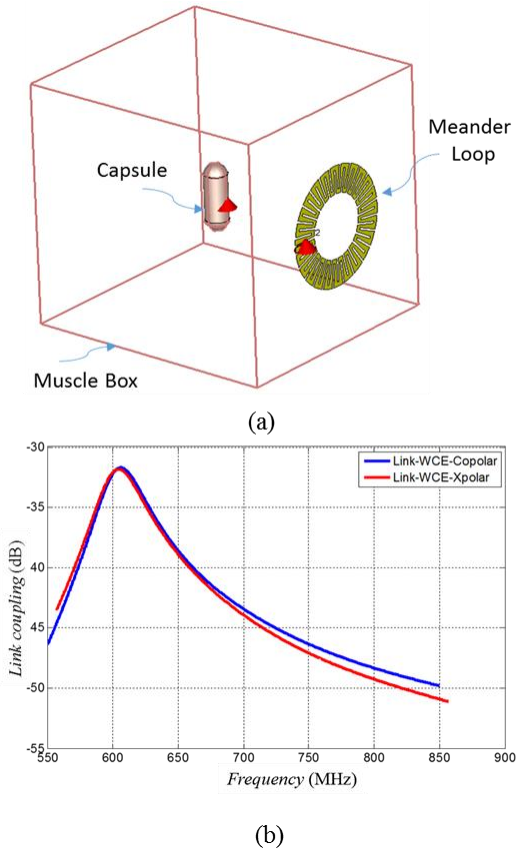

Fig. 9 a) Simulation scenario for the embedded capsule in the muscle tissues within the depth of 50 mm and the on body meander loop antenna b) Simulated coupling link for two different orthogonal polarizations of the on body antenna.

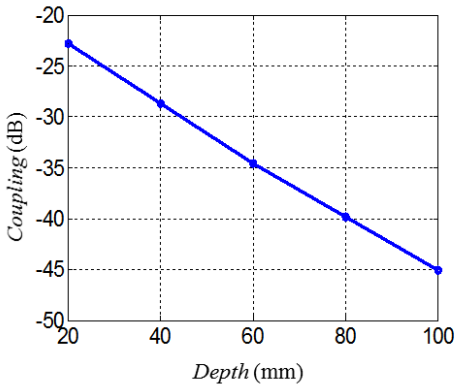

Fig. 10 Coupling link between the capsule antenna and the on-body antenna versus distance in the homogenous muscle tissue at 600 MHz; loss is a linear function of the distance with a slope of 2.6 dB/cm.

communicate with the implant antenna regardless of the capsule antenna orientation in parallel to the surface by using dual polar reader configuration. By increasing the implant antenna depth inside the muscle tissue, the amount of the coupling is reduced as shown in Fig. 10. The coupling reduces as a linear function of the depth, about 2.6 dB/cm at 600 MHz for the distances above 20 mm.

The backscatter communication uses bi-static, two side-by-side reader antennas, with orthogonal relative polarizations. A pair of side-by-side loop antennas with a gap distance of 6 mm are implemented as the reader to keep the implant antenna in the coverage regions of both reader antennas (see Fig. 11(a)). Relative rotation of 90 degrees is used to minimize the coupling between antennas for an increased dynamic range of the receiver and reduced probability of the receiver saturation. Fig. 11(b) shows the simulated and measured coupling between two side-by-side on body antennas. The simulation considered muscle tissue and the measurements use the liquid phantom.

The coupling link between the implant antenna and the on-body antennas is simulated to observe the effect of off-axis reader configuration in the bi-static setup. Fig. 11(c) shows the simulation scenario for the capsule within the depth of 50 mm. The maximum coupling link is reduced to -34.7 and -35.7 dB at 600 MHz, for each antenna, compared to -32 dB for on-axis usage in Fig. 9(b).

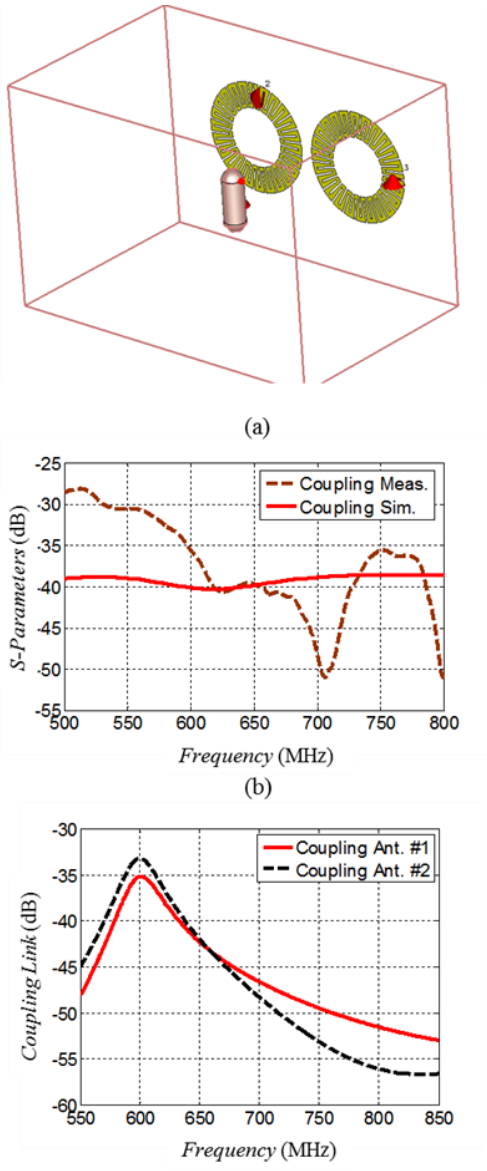

Fig. 11 a) Coupling link simulation scenario with two off-axis meander loop antennas. b) measured and simulated coupling between two side by side meander loop antennas with 90-degree relative rotations c) Coupling link between the capsule antenna and the two side by side loop antennas with 90-degree relative rotations. The capsule is placed off-axis within the depth of 50 mm.

VII. Backscatter Antenna Simulation and Measurements

The backscatter capsule antenna is simulated in the muscle tissue using the bi-static reader antenna configuration as shown in Fig. 11(a). The implanted antenna is simulated in parallel to the muscle surface. The mutual coupling between the reader antennas is computed for the switching modes of the implant antenna, i.e., open circuit (OC) and short-circuit (SC) states. In the simulations, the direct coupling between the on-body antennas is removed to discriminate the small changes caused by the switch states. Fig. 12 shows the simulated coupling between the reader antennas for the capsule at 50 mm depth. As shown, the maximum reflections occur at around 600 MHz by establishing the antenna resonance in the SC mode in which the reflection is -70 dB, and is reduced to -90 dB in the OC mode. The difference in the received signal is used to extract ΔRCS for data detection, i.e. 20 dB discrimination level is observed. The discrimination level is smaller for the frequencies away from the resonance. Thus, the expectation is that the backscatter works in off-resonance frequencies with degraded performance.

The amount of the peak reflection for different capsule depths is computed in the muscle tissue. The backscatter level (dB) reduces as a linear function of the distance with the amount of 5.2 dB/cm. The loss slope is approximately two times (in dB) of the path loss in the direct coupling link due to the round way

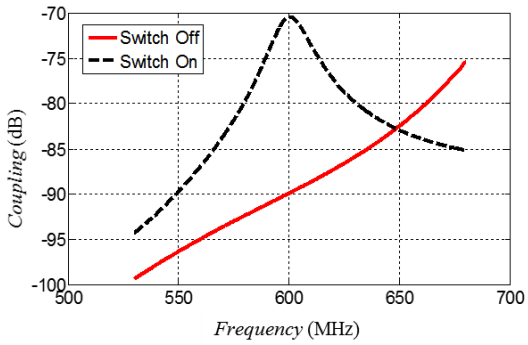

Fig. 12 Coupling between the reader antennas using SC and OC modes of the antenna switch by removing the direct coupling for the backscatter scenario in Fig. 11(a).

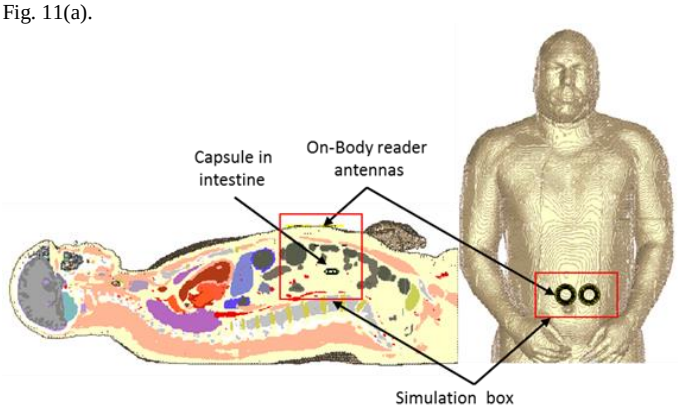

Fig. 13 Simulation model of the backscatter WCE in the anatomical model of the human body with the capsule inside the intestine and the on body reader antennas. The specified simulation box is the area used for EM computations

wave propagation.

The heterogeneous voxel model of the human body is used for electromagnetic computations (see Fig. 13). The model is

based on the data from the Visual Human Project® of the National Laboratory of Medicine (NLM) [32], in which the human body is represented by voxels with a spatial resolution of 1 mm. The voxels of the anatomical model are classified according to their different dielectric material properties. Thirty-two different types of biological tissues are defined in the model. The numerical simulations are conducted using time domain solver of CST MWS. The frequency-dependent dielectric properties of the human tissues are used. The reader antennas are placed on the body surface in the abdomen area, and the capsule is in parallel to the body surface. The simulation region is limited to the capsule and reader antenna areas as specified in Fig. 13, to reduce the simulation time and memory. The boundary for the selected region is a perfectly matched layer (PML), to prevent wave propagation from the side walls of the region into the body, except for the on body side which is an open boundary.

The coupling value between the capsule antenna and the on body antennas is computed in which for the capsule within the depth of 50 mm, the coupling is -34.1 and -35.7 dB and the capsule antenna resonance is shifted to 625 MHz. The frequency shift compared to the muscle scenario is related to the antenna loading with different tissues.

The backscatter link is computed by using the reader antennas in the Voxel simulations. The attempt is to monitor the frequencies for which the reflections are maximum and the level of the reflections. It is observed that the backscatter frequency is maximum at about 610 MHz with the maximum reflection level of -70 dB for the depth of 50 mm. The backscatter coupling increases to -62 dB for 30 mm depth. We note that the final antenna implementation in the biological tissues might be different from the simulations due to the antenna loading with the tissues and the antenna integration with the electronics inside the capsule shell. The main effect is the change in the resonance frequency of the antenna. The point with the capsule antenna is that the backscatter reflections can be significant for about 24 MHz frequency deviation compared to the optimum frequency with a maximum of 5 dB degradations. The optimal frequency can be found using the frequency scan option applied to the reader device.

The capsule antenna has been manufactured on a flexible Kapton dielectric with a thickness of 50 microns. The electronic board is manufactured on a circular FR4 substrate and includes an RF switch UPD5713TK controlled by a data source of 1 and 5 Mbps. The RF switch is used to connect or disconnect the resonance state of the antenna. The antenna and the electronics are integrated inside a glass shell. Fig. 14(a), (b) shows the manufactured antenna prototypes. Fig. 14(c), (d) shows the schematic circuit of the switch and the data source which is a periodic {0,1} sample provided by DSC1001 oscillator circuit.

The backscatter communication system is measured by using the capsule inside the liquid phantom. A large plastic container of size 30×30×35 cm^3 with the wall thickness of 1.2 mm is filled with the liquid. The bi-static reader antenna configuration is

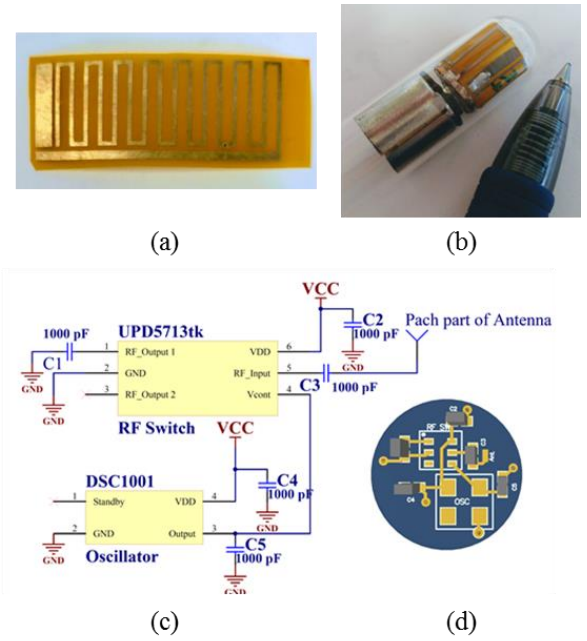

Fig. 14 Manufactured antenna prototypes and the system electronic boards a) planar antenna b) conformal antenna with the capsule shell, battery and the electronics. c) schematic diagram of the switch board and the control using periodic data generator d) PCB layout with the specified antenna connection.

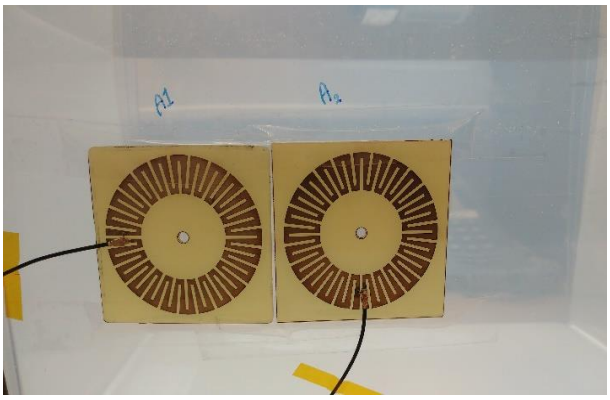

Fig. 15 Reader antenna placement on the liquid phantom container.

used for transmitting and receiving the signals (Fig. 15). One reader antenna is connected to a signal generator as the transmitter source, and the next antenna is connected to a spectrum analyzer to monitor the spectrum of the backscatter signals. A thin cotton string is used to hang the capsule antenna in the liquid phantom to minimize the effects of any other capsule holders. The capsule's transmitting data is a periodic sequence of {0, 1} with the speed of 1 Mbps. The spectrum of the periodic data becomes two spikes with a shift of 1 MHz around the reader tone signal. The main feature of using the periodic data, in the test process, is to discriminate the data spikes from the coupling tone signal for easy monitoring and measurement of the backscatter data signal level. The transmitter frequency is scanned around the design frequency (600 MHz) to find the frequency for which the backscatter signal is significant. Fig. 16(a) shows the measured spectrum at the receiver antenna. The central peak signal is the leakage from the transmitter to the receiver and has no information. The two 1 MHz shifted spikes that are clear from the central coupling

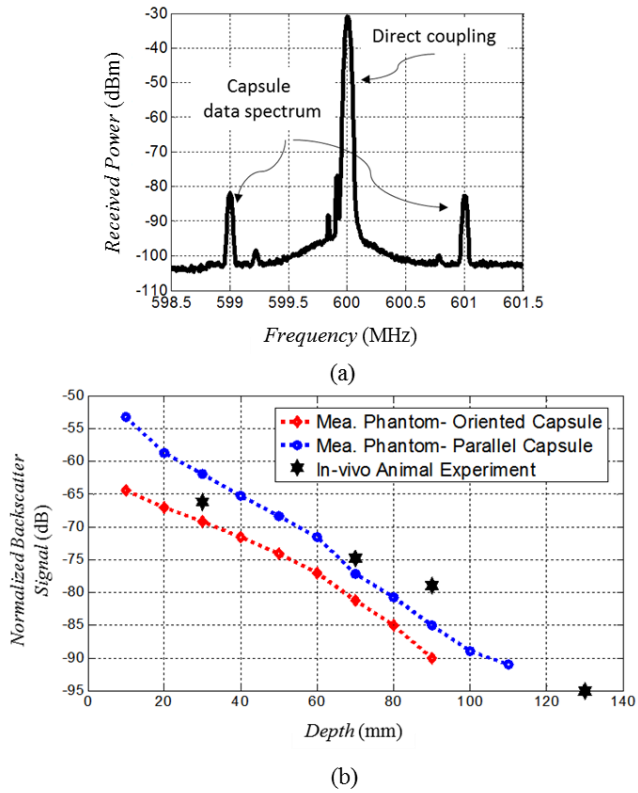

Fig. 16 Received signal spectrum in the backscatter link using bi-static reader configuration in the presence of the capsule antenna with periodic data stream at 1 Mbps. The direct coupling appears as a DC signal after demodulation and the spectrum's sidelobes indicate the data signal power b) measured data signal level (dB) normalized to the transmitter power in the phantom and in-vivo animal test.

are the results of switching and contains the spectrum of the capsule's data. Without switching the central coupling is the only visible signal in the spectrum analyzer. We note that by using the random data, the data spikes will be distributed around the main coupling signal up to ±1 MHz. In this case, finding the visible peak data signal as in Fig. 16(a) is not possible, so the backscatter link evaluation is difficult.

The backscatter link quality is evaluated by monitoring the peak power of the shifted spectrum for different depths and orientations of the capsule antenna. The applied power in the measurements is 20 dBm, the cable loss is 2 dB for each transmitter and receiver cables. By removing the cable's loss and by scaling the accepted power to 1 mW (0 dBm) the measured backscatter signal level (dBm) for different capsule depths is shown in Fig. 15(b). The illustrated backscatter signal levels are related to the backscatter round way link loss. For the capsule in parallel to the surface of the container, the backscatter coupling at 50 mm depth is -69 dB, while in the simulations it was -70 dB. The average measured backscatter path loss versus depth, for the depths beyond 20 mm, can be interpolated as a linear decay function of 3.7 dB/cm. The path loss has faster decay nearby the surface due to the extreme near-field coupling.

By rotating the capsule with almost 60 degrees relative to the container surface, non-parallel to surface condition, the

backscatter level is reduced by 12 dB in the depths close to the surface due to the polarization mismatch. The polarization mismatch is less within further depths due to the wave depolarization by propagation through the medium, and the path loss is reduced by 5 dB in 80 mm depth. By using the capsule in a perpendicular orientation relative to the surface, the coupling reduces by 15 dB compared to the parallel conditions. In this orientation, it is preferred to change the placement of the reader antennas to illuminate the capsule from different orientations thus compensate for the polarization mismatch. This can be done using multiple reader antennas in the final implementation setup and switching among the transceiver antennas for optimum backscatter signal reception.

The maximum accessible depth for the backscatter WCE considering a typical receiver sensitivity of -90 dBm, and maximum transmitter power of 1 mW (0 dBm) is 10 cm for the optimum capsule-reader orientations. By considering the polarization mismatch of 10 dB (due to the capsule rotation) and a link margin of 10 dB, the transmitter power of 100 mW can provide reliable link connectivity with the capsule at 10 cm. The applied power is in the acceptable range for RF safety, SAR.

We note that using high power in transmission may not always be an optimum way of connectivity because of the direct coupling to the receiver that can saturate the receiver system. The leakage to the receiver can be further managed and reduced by applying a portion of the transmitted power into the receiver electronics before LNA and phase/amplitude tuning for canceling the coupled power between the antennas. This requires accurate phase tuning and closed-loop control approach.

The reader system is implemented using software defined radio (SDR), USRP N210 and SBX-40 radio module from National Instrument (NI). MATLAB Simulink is used to communicate with the SDR. Fig. 17(a) shows the photograph of the measurement setup. The MATLAB program is used to tune the transmitter frequency and the receiver/ transmitter gains. The receiver process diagram is shown in Fig. 17(b). In the receiver, the direct coupling appears as dc signal after demodulation that is removed using a dc blocker with IIR filter. The signal demodulation is conducted by filtering the sampled signals using raise-cosine filter with roll-off factor 0.5, and then the course and fine frequency compensations are applied for the synchronization and timing recovery. Real-time data reading is tested using the SDR module in the phantom experiments. A capsule with the switching rates of 1 and 5 Mbps is measured. It is observed that the levels of the two side spectrums are symmetric in the above given bandwidth, that results in a non-distorted channel of the backscatter in the biological medium using both rates. Thus the reader system does not need to use a matched filter to compensate for the distortions. The implemented USRP reader can communicate with the capsule for the depths up to 10 cm by the accepted antenna power of 16 dBm (39.8 mW). Fig. 18(a) shows a sample of the demodulated signal in the receiver for I & Q channels for the capsule at depth 7 cm. As shown, the data bits can be easily extracted from the demodulated signal. Fig. 18(b) shows the data signal after raised cosine filtering. The constellation diagram of the data signal after time recovery and synchronization process is shown Fig. 18(c).

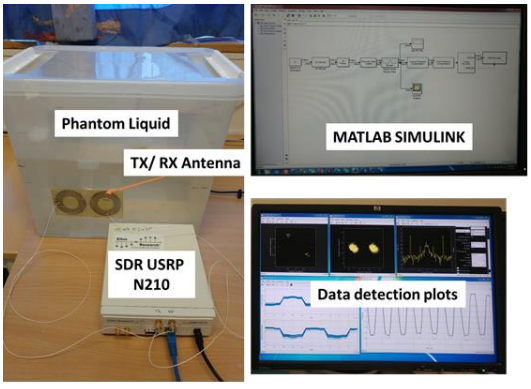

(a)

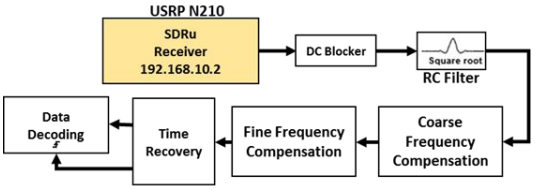

(b)

Fig. 17 a) Photograph of the measurement setup b) receiver process for synchronization and data recovery

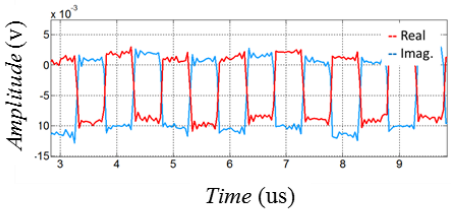

(a)

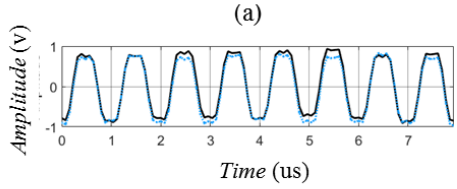

(b)

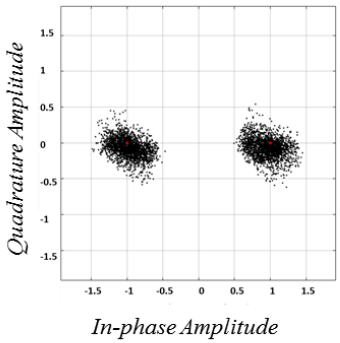

(c)

Fig. 18 a) Demodulated backscatter data signal using SDR USRP N210 and SBX-40 radio module for R_b=1 Mbps in I & Q channels b) data signal after RC filter c) constellation diagram of the data.

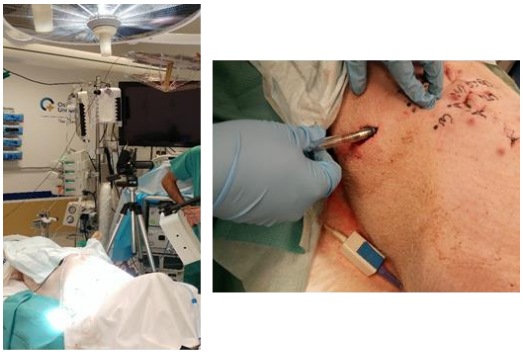

(a) (b)

Fig. 19 a) Photograph of OR for animal experiments at the Intervention Center, Oslo University Hospital b) illustration of the capsule antenna insertion into the animal abdomen through a small incision for in-vivo backscatter measurements.

The receiver sensitivity is calculated for the SBX-40 radio assuming OOK demodulation [33]. The receiver noise figure (NF) is 5 dB, the required energy per bit to the noise power spectral density (E_b/N_o) is 14 dB for BER=10^{-6}. The IF bandwidth of the receiver is 25 MHz and the data rates are 1 and 5 Mbps. The data filter bandwidth is raised cosine with roll-off factor 0.5. The calculated receiver sensitivity for the data rate of 1 Mbps is -92 dBm and for 5 Mbps is -87 dBm. We note that the receiver sensitivity can be improved by using an external LNA with lower NF or accepting lower BER=10^{-3}. Referring to Fig. 16(b) we can calculate the communication depth based on the calculated receiver sensitivity for the given data rates by applying 1 mW of the power.

The in-vivo animal experiments are conducted on a pig weighing 61 Kg. To evaluate and compare the performance of the capsule in an environment similar to that of the human body, the pig is prepared under a general anesthetic in the operating room of the Intervention Centre, Rikshospitalet, Oslo University Hospital, Norway. The center has accreditation for conducting animal experiments. All the experiments are performed in strict compliance with laws regarding Ethic standards and humane treatment of animals. Because this animal was alive and all of its organs were operating normally, the experimental conditions were virtually identical to the conditions expected in a human body.

First, the capsule is inserted through an incision in the animal abdomen and placed close to the abdomen surface at about 3 cm depth (see Fig. 19(b)). The transmitter frequency is swept around 600 MHz to find the frequency for which the maximum backscatter is observed. The optimum backscatter frequency is found at around 597 MHz, instead of the designed 604 MHz. The reason is the different material surrounding the capsule in the in-vivo experiments compared to the liquid phantom and muscle/Voxel tissue simulations. Even though we can read the capsule signal at 604 MHz, but the backscatter signal level is 2 dB less than the optimum read frequency.

The capsule device is placed in more depths in the abdomen of the animal among the intestine tissues on the external surface of the intestine. We did not cut the small intestine for inserting the capsule as it might place the animal in an unstable condition. The incisions are closed to prevent any leakage of the signal through the holes. Similar to the phantom experiments, the reader antennas are placed on the surface of the abdomen above the approximate location of the capsule. The placement and orientations of the capsule are not well under control due to movements of the intestine and the capsule during the experiment. So it is difficult to evaluate the exact depth and rotation of the capsule. Trials are conducted to measure approximate depth. The measured results are qualitative and show the feasibility of wireless backscatter connectivity in the in-vivo tests. The reader antennas are placed and moved on the abdomen surface to obtain the backscatter signal from the capsule. The antennas are not necessarily in a flat surface due to the shape of the abdomen and the elasticity of the tissues. The rotation of the reader antennas is changed to obtain the maximum data signal level, i.e., the reader polarization is manually tuned. The received power is directly visualized using the spectrum analyzer by transmitting 20 dBm of the power in which 4 dB is related to the loss of the cable. The backscatter signal level by scaling the accepted power to 0 dBw, is depicted in Fig. 16(b) for the approximate measurement depths at 30, 70, 90, 130 mm. The in-vivo signal level is approximately (±5 dB) matched to the liquid phantom measurements. The deviation is mainly because of the unknown orientation of the capsule, the reader antennas' placement on the animal body, and the accuracy of the in-vivo setting

VIII. Conclusion

Radio frequency backscatter is used for high data rate deep implant wireless communications. The backscatter eliminates the power-hungry transmitter unit from the implant device and can save several 10's of mW power in the implant unit that makes high data rate and continues connectivity feasible for improved visualization of the small intestine. To succeed with the deep implant backscatter, the implant antenna and the external reader antennas are precisely designed for the biological medium. Loop antenna geometry is applied to both the internal and external antennas.

The capsule antenna of length 11.5 mm and diameter 9 mm, has a meander loop geometry with a capacitive feed mechanism for generating a resonance frequency with less influence from the surrounded biological tissues. The antenna is fabricated using a flexible substrate material and is integrated into the perimeter of a cylindrical capsule device. The antenna resonance is at 600 MHz, and the radiations are dual polar. The antenna RCS is controlled using active switching of the antenna modes.

Bi-static on body antennas are designed and used for wireless communications. The reader antennas have meander loop geometry to reduce the overall size and are self-matched at 600 MHz frequency. The reader antennas are linear polarized and are used in a side-by-side configuration to communicate with the implant capsule. Orthogonal polarizations reduce the coupling between the nearly spaced reader antennas. The meander loop antennas have the maximum radiation in their main axes direction and can forward the power to the internal body with an acceptable level of SAR.

The backscatter link is established using the bi-static reader.

The link is computed using numerical simulations and is measured in a liquid phantom. The backscatter path loss versus depth is extracted by implementing a periodic data stream in the capsule device. A linear path loss as a function of depth is obtained for both phantom liquid and homogenous muscle tissues. The computed average backscatter path loss in the muscle tissue is 5.2 dB/cm and in the liquid phantom mimicking the average body tissues is 3.75 dB/cm. The backscatter WCE is tested in the in-vivo animal experiments to validate the operation of the system. We have shown a very consistent link for the depths up to 13 cm with a moderate reader power up to 250 mW and data rates of 1 and 5 Mbps. The power level shall be changed considering the received signal level to minimize the SAR. In the in-vivo test, we use a frequency scan around the design frequency to compensate for the possible resonance frequency shift of the implant antenna due to the bio-material loading. A communication system is realized using SDR and the demodulated data signals and constellation diagrams are presented.

ACKNOWLEDGMENT

The authors thank surgeon J. Bergsland and the surgical team for performing the animal experiment at the Intervention Center, Oslo University Hospital.

REFERENCES

[1] R. B. Green, "The general theory of antenna scattering," *Report No. 1223-17, Electron Science Laboratory*, Columbus, OH, Nov, 1963.

[2] P.V Nikitin, K.V.S. Rao, "Theory and measurement of backscattering from RFID tags," *IEEE Ant. Propag. Mag.*, vol 48 , no.6, pp. 212 – 218, Dec. 2006.

[3] M. Buettner, B. Greenstein, A. Sample, J. R. Smith, and D. Wetherall, "Revisiting smart dust with RFID sensor networks," *in Proc2008 ACM Workshop on Hot Topics in Networks*, Oct. 2008.

[4] R. Correia and N. B. Carvalho, "Ultrafast backscatter modulator with low-power consumption and wireless power transmission capabilities," *in IEEE Microwave and Wireless Components Letters*, vol. 27, no. 12, pp. 1152-1154, Dec. 2017.

[5] A. Hasanvand, A.Khaleghi, I. Balasingham "Coherent query scheme for wireless backscatter communication systems with single tag", *EURASIP Journal on Wireless Communications and Networking*, vol. 2018, 2018.

[6] S. Naderiparizi, M. Hessar, V. Talla, S. Gollakota, and J. R. Smith. "Towards batteryfree hd video streaming", *15th USENIX Symp. On Networked Systems Design and Implementation (NSDI)*, April 9-11, 2018, Renton, WA, USA.

[7] Vikram Iyer, Vamsi Talla, Bryce Kellogg, Shyamnath Gollakota, Joshua R Smith, "Inter-technology backscatter: towards internet connectivity for implanted devices" *In proceedings of the 2016 ACM SIGCOMM Conference (SIGCOMM 2016)*, August 2016.

[8] H. Aubert, "RFID technology for human implant devices" *Comptes Rendus Phys.*, vol. 12, no. 7, pp. 675–683, Sep. 2011.

[9] J. S. Besnoff and M. S. Reynolds, "Near field modulated backscatter for in vivo biotelemetry," *2012 IEEE International Conference on RFID (RFID)*, pp. 135–140, May. 2012.

[10] E. Moradi et al., "Backscattering neural tags for wireless brain-machine interface systems," *IEEE Trans. Antennas Propag.*, vol. 63, no. 2, pp. 719– 726, Feb. 2015.

[11] A. Sample, D. Yeager, P. Powledge, and J. Smith, "Design of a passively powered, programmable sensing platform for UHF RFID systems," *in Proc. 2007 IEEE International Conference on RFID*, pp. 149–156

[12] Stewart J. Thomas, Jordan S. Besnoff, and Matthew S. Reynolds. "Modulated backscatter for ultra-low power uplinks from wearable and implantable devices" *In Proceedings of the 2012 ACM workshop on Medical communication systems (MedCOMM '12)*. ACM, New York, NY, USA, 1-6.

[13] H. Cao, V. Landge, U. Tata, Y.-S. Seo, S. Rao, S.-J. Tang, H.F. Tibbals, S. Spechler, and J.-C. Chiao, "An implantable, batteryless and wireless capsule with integrated impedance and ph sensors for gastroesophageal reflux monitoring," *IEEE Trans. on Biomedical Engineering*, vol. 59, no. 11, pp. 3131-3139, 2012.

[14] J. Riistama, E. Aittokallio, J. Verho, and J. Lekkala, "Totally passive wireless biopotential measurement sensor by utilizing inductively coupled resonance circuits," *Sens. Actuators A, Phys.*, vol. 157, no. 2, pp. 313–321, Feb. 2010.

[15] R. Lodato, V. Lopresto, R. Pinto, and G. Marrocco, "Numerical and experimental characterization of through-the-body UHF-RFID links for passive tags implanted into human limbs," *IEEE Trans. Antennas Propag.*, vol. 62, no. 10, pp. 5298–5306, Oct. 2014.

[16] H. N. Schwerdt *et al.*, "A fully passive wireless microsystem for recording of neuropotentials using RF backscattering methods," *J. Microelectromech. Syst.*, vol. 20, pp. 1119–1130, Oct. 2011.

[17] S.Gabriel, R.W.Lau and C.Gabriel: The dielectric properties of biological tissues: II. Measurements in the frequency range 10 Hz to 20 GHz, *Phys. Med. Biol. 41 (1996)*, 2251-2269.

[18] Technical and operating parameters and spectrum use for short-range radio communication devices, International Telecommunication Union. [Online]. Available: www.itu.int/pub/ R-REP-SM.2153-2- 2011.

[19] ETSI EN 301 839-1, European Telecommunications Standards Institute, 2007. Online Available: http://www.etsi.org/deliver /etsi_en/ 301800_301899/ 30183901/01.03.01_60/en_ 30183901v010301p.pdf

[20] Federal Communications Commission, 47 CFR 95.601-95.673 Subpart E, 1999. [Online]. Available: http://wireless.fcc.gov/services/index.htm?job =operations&id=medical_implan

[21] A. Khaleghi, I. Balasingham, "Power coupling for conceptual antennas in medical implant applications", *11th European Conference on Antennas and Propagation (EUCAP) 2017*, 19-24 March 2017, Paris France

[22] Harrington, R. F.. "Effect of antenna size on gain, bandwidth, and efficiency" J. Res. Nat. Bur. Stand 64 , no. 1 (1960): 1-12.

[23] P. V. Nikitin and K. V. S. Rao "Theory and measurement of backscattering from RFID tags," *IEEE Antennas Propag. Mag.*, vol. 48, no. 6, Dec. 2006

[24] A. Bletsas, A. G. Dimitriou, and J. N. Sahalos "Improving backscatter radio tag efficiency," *IEEE Trans. Microw. Theory Techn.*, vol. 58, no. 6, pp. 1502–1509, Jun. 2010.

[25] S. Ebrahimi-Asl, M. Tayeb Ghasr, M. J. Zawodniok "Design of Dual-Loaded RFID Tag for Higher Order Modulations" *IEEE Trans. Microw. Theory and Techn.*, vol. 66, Iss. 1, pp. 410 – 419, Jan. 2018

[26] L. A. Muth, C. M. Wang, and T. Conn, "Robust separation of background and target signals in radar cross section measurements," *IEEE Trans. Instrum. Meas.*, vol.54, no.6, pp. 2462-2468, 2005.

[27] C.C.Yen , A. E. Gutierrez, D. Veeramani, D. Weide, "Radar cross-section analysis of backscattering RFID tags" *IEEE Antennas and Wireless Propagation Letters*, vol. 6 , pp. 279 – 281, 2007.

[28] R.Chavez-Santiago, A. Khaleghi, I. Balasingham "Matching layer for path loss reduction in ultra wideband implant communications" *Engineering in Medicine and Biology Society (EMBC), 36th Annual International Conference of the IEEE*, pp. 6989-6992, 2014.

[29] T. Yousefi and R. E. Díaz, "Pushing the limits of radiofrequency (RF) neuronal telemetry," *Sci. Rep.*, vol. 5, p. 10588, Jun. 2015.

[30] A. Khaleghi, I. Balasingham, R. Chávez-Santiago "An ultra-wideband wire spiral antenna for in-body communications using different material matching layers", *Engineering in Medicine and Biology Society (EMBC), 2014 36th Annual International Conference of the IEEE*, pp. 6985-6988, Aug. 2014.

[31] RF exposure evaluation report for sproutling smart sleep wearable-hub, Model Number FNF59, FCC ID: PIYFNF59-17A5H, Report No. 17020160HKG-001, available online, https://fccid.io/PIYFNF59-17A5H/RF-Exposure-Info/SAR-3562352.

[32] E. Gjonaj, M. Bartsch, M. Clemens, S. Schupp, and T. Weiland, "High-resolution human anatomy models for advanced electromagnetic field computations," *IEEE Trans. Magn.*, vol. 38, no. 2, pp. 357-360, Mar. 2002.

[33] Calculating the Sensitivity of an ASK Receiver, *APPLICATION NOTE 2815*, Maxim Integrated, Nov 05, 2003.

Ali Khaleghi (M'02, SM'14) received Ph.D. in Physics from the University of Paris XI, Paris, France in 2006. From 2006 to 2007, he was postdoc at the Institute d' Electronique et de Télécommunications de Rennes (IETR), France. From 2008 to 2009 was postdoc at the Intervention Center (IVS), Oslo University Hospital, Norway. From 2010 to 2015, he was assistant professor in the Electrical and Computer Engineering Department at K. N. Toosi University of Technology (KNTU), Tehran, Iran. He obtained several research and industrial grants during his career at KNTU. He established Wireless Terminal Test Lab (WTT) at KNTU. He distinguished as the best researcher of KNTU in 2013. From, 2015, he is an adjunct professor at KNTU and scientist at the Norwegian University of Science and Technology (NTNU) and Oslo University Hospital. His research field is on antennas and waves propagation, wireless communications, electromagnetic compatibility (EMC), measurement techniques and bio-electromagnetics. He has authored over 90 journal and full conference papers and hold 4 international patents. He is a Senior IEEE Member.

Aminolah Hasanvand received MSc in electronics and telecommunication engineering from the University of Tabriz, Tabriz, Iran, in 2007. He has 8 years of experience in wireless communications.
He is Ph.D. student at the electrical engineering department at K. N. Toosi University of Technology, Tehran, Iran. His main research interests include wireless backscatter communications, passive RFID, in-body wireless sensor communication systems, and software defined radio implementations.

Ilangko Balasingham (M'98, SM'11) received the M.Sc. and Ph.D. degrees from the Department of Electronics and Telecommunications, Norwegian University of Science and Technology (NTNU), Trondheim, Norway in 1993 and 1998, respectively, both in signal processing. He performed his Master's degree thesis at the Department of Electrical and Computer Engineering, University of California Santa Barbara, USA. From 1998 to 2002, he worked as a Research Engineer developing image and video streaming solutions for mobile handheld devices at Fast Search & Transfer ASA, Oslo, Norway, which is now part of Microsoft Inc. Since 2002 he has been with the Intervention Center, Oslo University Hospital, Oslo, Norway as a Senior Research Scientist, where he heads the Wireless Sensor Network Research Group. He was appointed as a Professor in Signal Processing in Medical Applications at NTNU in 2006. For the academic year 2016/2017 he was Professor by courtesy at the Frontier Institute, Nagoya Institute of Technology in Japan. His research interests include super robust short range communications for both in-body and on-body sensors, body area sensor network, microwave short range sensing of vital signs, short range localization and tracking mobile sensors, and nanoscale communication networks. He has authored or co-authored over 225 journal and conference papers, 7 book chapters, 42 abstracts, 6 patents, and 20 articles in popular press. Ilangko has given 16 invited/ keynotes at the international conferences. In addition, he is active in organizing conferences (Steering Committee Member of ACM NANOCOM 2018-2021; General Chair: the 2019 IEEE Int. Symposium of Medical ICT, the 2012 Body Area Networks (BODYNETS) conference; TPC Chair of the 2015 ACM NANOCOM) and editorial board (Area Editor of Elsevier Nano Communication Networks 2013-unti now). He is a Senior IEEE Member.